Multi-Stage Wavelength Locking in a 4 × 4 Silicon Electro-Optic Switch Based on Dual-Ring Resonators

Qingming Zhu, Xinhong Jiang, Ruiyuan Cao, Hongxia Zhang, Ciyuan Qiu, and Yikai Su
State Key Laboratory of Advanced Optical Communication Systems and Networks,
Department of Electronic Engineering, Shanghai Jiao Tong University, Shanghai 200240, China
Author e-mail address: yikaisu@sjtu.edu.cn

Abstract: *We experimentally demonstrate a multi-stage wavelength locking scheme based on saddle point searching in a dual-ring based 4×4 electro-optic switch. Three-stage switching elements can be aligned to the signal wavelength with initial ≲2-nm wavelength misalignments.*
Keywords: *Switching Technologies, Subsystems and Advanced Functionality*

I. Introduction

Driven by the ever-increasing global data traffic, optical switching has emerged as a promising candidate to provide high switching capacity, low signal latency, and low power consumption [1]. Typically, a wavelength division multiplexed (WDM) switch fabric is achievable with multiple single-wavelength switching layers [2]. Therefore, resonant devices can be used as the basic building blocks of optical switches. Furthermore, resonant devices may offer several key advantages including compact footprint, relatively low power consumption, and sharp spectral selectivity [3]. The main shortcoming of resonator-based switches is their high sensitivity to fabrication errors and temperature variations. To solve the problem of wavelength misalignments in a large-scale switch fabric, automated wavelength locking of the resonators is needed [3]. Most of the existing automated wavelength locking methods were demonstrated in optical modulators and filters (e.g., [4], [5]), which may not work for switching elements with dual inputs. Recently, we proposed a saddle-point-searching (SPS) algorithm for the wavelength locking of dual-input switching elements based on dual-ring resonators [6]. The SPS algorithm was later optimized to enable the wavelength locking over a full free spectral range (FSR) [7]. However, the improved SPS algorithm was only demonstrated in a single 2 × 2 switching element.

In this paper, we present an extended experimental demonstration of the improved SPS algorithm in a dual-ring based 4 × 4 silicon electro-optic (EO) switch. Compared to the demonstration in [7], a multi-channel control subsystem is required, together with optimizations of the locking parameters for achieving enhanced fabrication tolerance. The 4 × 4 switch employs Benes architecture and therefore consists of three-stage switching elements. The control subsystem can lock the three-stage switching elements to the signal wavelength, provided that the initial wavelength misalignments are less than 2 nm.

II. Device Structure and Subsystem Configuration

Fig. 1(a) shows the schematic diagram of the 4 × 4 switch and the control sub-system. The switch comprises of six switching elements. For each switching element, its resonance wavelength is affected by fabrication errors and temperature variations, hence a feedback loop is used to realize wavelength locking. Specifically, the monitored photocurrent signal from the switch chip is amplified by a trans-impedance amplifier (TIA), and then sent to a digital signal processor (DSP). With the SPS-based wavelength locking algorithm, a thermo-optic (TO) tuning signal with a controlled tuning power is applied to the switching element. In addition, the on/off control of each switching element is realized by the subsystem. Fig. 1(b) shows the device structure of the switching element. The device contains two coupled ring resonators, and each ring resonator is integrated with a micro-heater, a p-i-n diode, and a directional coupler for power monitoring. Germanium photodiodes are also integrated to detect the monitored optical signals.

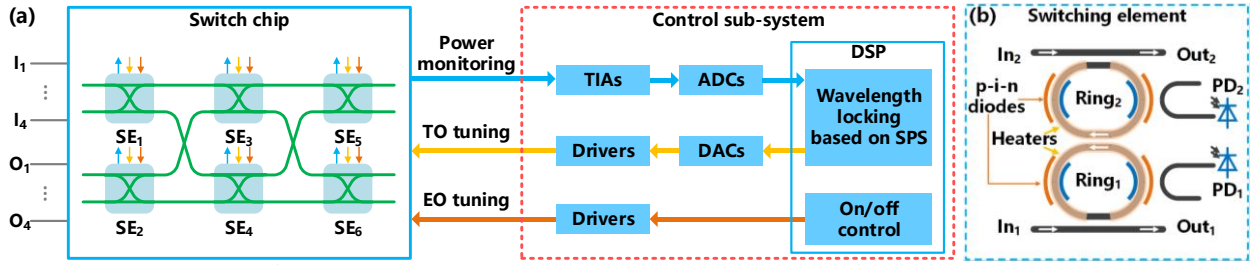

Fig. 1. (a) Schematic diagram of the 4 × 4 switch and the control sub-system. (b) Device structure of the switching element. SE: switching element. ADCs: analog-to-digital converters. DACs: digital-to-analog converters.

III. Device Design, Fabrication, and Packaging

The device layouts of the 4 ×4 silicon EO switch and the switching element are shown in Fig. 2(a) and (b), respectively. The switch operates in O band. It consists of six switching elements, two crossings, and eight grating couplers spaced by 127 μm. The footprint of the 4 ×4 switch is 4.0 mm × 1.4 mm. In the switching element, each ring resonator has a radius of 10 μm, and correspondingly an FSR of 6 nm at 1310 nm. The gap parameters are gap_1 = 220 nm, gap_2 = 370 nm, gap_3 = 250 nm. The two p-i-n diodes in each switching element are controlled by a same EO tuning signal to reduce the device footprint and the number of control signals. The device was fabricated through a one-to-one run in IME Singapore. Afterwards, electrical packaging and optical packaging were performed in order, with the photographs shown in Fig. 2(c) and (d). All the metal pads of the switch are connected to the control PCB through wire bonding. A 10-channel 127-μm-pitch fiber array based on vertical coupling is used to couple the lights into and out of the switch. The fiber array is mounted on the switch chip by using ultra-violet (UV) light curable adhesive. The coupling loss is ~5 dB/facet.

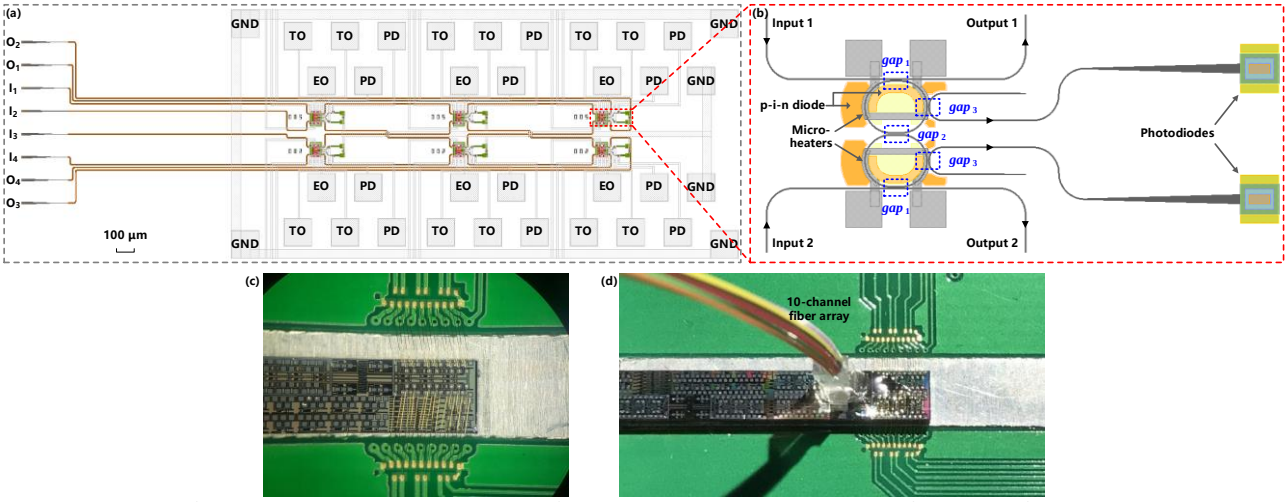

Fig. 2. (a) Layout of the 4 ×4 silicon EO switch. (b) Layout of the switching element. (c) Photograph of the switch after electrical packaging. (d) Photograph of the switch after optical packaging. PD: photodiode.

IV. Experimental Results

The experimental setup is presented in Fig. 3. A continuous wave light at 1306 nm from an O-band laser source is adjusted by a polarization controller to be TE-polarized, and then injected into the switch chip. The initial resonance wavelengths of the ring resonators are in the range of 1304−1305 nm. In the experiment, we tested one input port and one output port at a time. The output light is split into two parts, for Labview-controlled power monitoring and real-time power monitoring, respectively. In the control subsystem, there are twelve TIAs for amplifying the photocurrent signals. The amplified signals are sampled by twelve 10-bit ADCs (TLC1543), with the sampled data sent into a commercial single-core processor (STM32F407) operating at 168 MHz. Both the wavelength locking algorithm and the on/off control are realized in the processor via C code. To achieve the TO tuning operations, twelve TO tuning signals are generated by 8-bit DACs (TLC5628) and the following drivers. To realize the fast switching, the processor also produces six square-wave drive signals, with their 10%−90% switching times of ~2 ns. To test the wavelength locking algorithm in different optical paths, the processor is also connected to a computer that determines the routing state of each switching element. The wavelength locking algorithm is based on our previously reported algorithm [7], which consists of a coarse searching process and three fine searching processes. However, there are several differences between the two algorithms in terms of the locking parameters. Firstly, the new algorithm supports multiple locking channels, i.e., it can control all the twelve ring resonators in order. Secondly, the thermal feedback control period is set to 100 μs, which is twice that of our previously reported algorithm to reduce more noise in the sampled signal. Thirdly, with the larger scale of the switch,

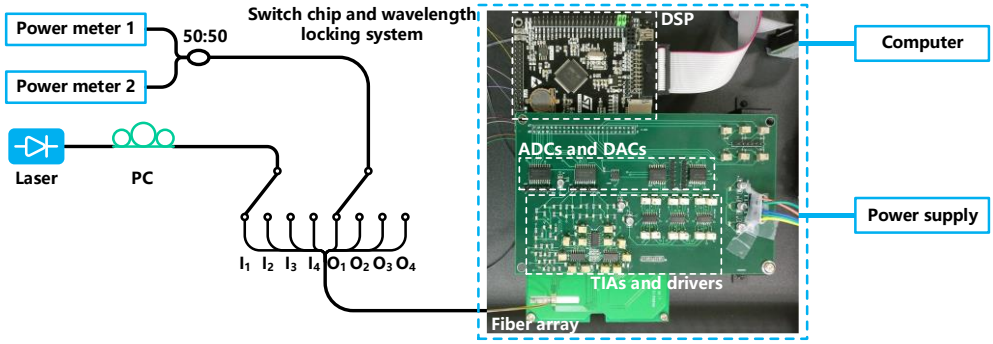

Fig. 3. Experimental setup. PC: polarization controller.

more fabrication errors are induced. To improve the fabrication tolerance, the TO tuning ranges in the fine searching processes are set to three or four times as large as that in [7].

The wavelength locking is demonstrated for three different optical paths of the switch, with the optical paths and the measured transmission spectra shown in Fig. 4(a), (b), and (c), respectively. For each optical path, the three cascaded switching elements in the path are aligned to the signal wavelength, whereas the other switching elements are not thermally tuned. Hence, the optical power at the designated output port is maximized. For example, in Fig. 4(a), the input light is sent into I_1 port, and the switching elements SE_1, SE_3 and SE_6 are locked to 1306 nm, therefore the optical power at O_4 port is maximized. This switch exhibits high insertion losses and severe crosstalk, because the gap parameters of the dual-ring resonators were not properly designed. With the wavelength locking, the minimal operation bandwidth among the three optical paths is 0.25 nm. Fig. 4(d) shows the fast switching results measured after the wavelength locking. The routing states of SE_2, SE_4 and SE_5 are simultaneously tuned between the bar state and the cross state by EO tuning. An extinction ratio of 25 dB at O_1 port is therefore achieved, and the 10%–90% switching times for the rise edge and the fall edge are 19 ns and 13 ns, respectively.

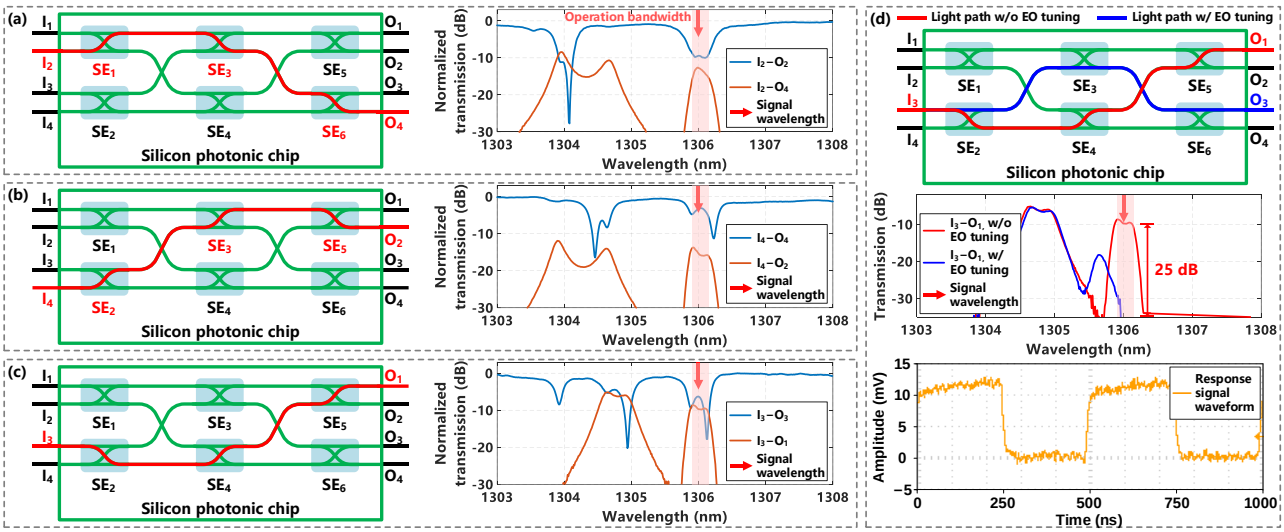

Fig. 4. (a)–(c) Three different optical paths (red lines) and the transmission spectra measured after wavelength locking. (d) Routing configuration, transmission spectra w/ and w/o EO tuning, and response signal waveform.

V. Conclusions

We experimentally demonstrated the three-stage wavelength locking in a dual-ring based 4 ×4 silicon EO switch. By using a multi-channel control subsystem and an optimized SPS algorithm, the three-stage switching elements are aligned to the signal wavelength with the initial wavelength misalignments of ≤ 2 nm.

Acknowledgment

This work was supported in part by the National Natural Science Foundation of China under Grant 61860206001/61835008, and in part by the Science and Technology Commission of Shanghai Municipality under Grant 16XD1401400/17500710900.

References

[1] G. I. Papadimitriou, C. Papazoglou, and A. S. Pomportsis, “Optical switching: Switch fabrics, techniques, and architectures,” J. Lightw. Technol., vol. 21, pp. 384-405, February 2003.

[2] J. M. Elmirghani, and H. T. Mouftah, “Technologies and architectures for scalable dynamic dense WDM networks,” IEEE Commun. Mag., vol. 38, pp. 58-66, February 2000.

[3] Y. Li, Y. Zhang, L. Zhang, and A. W. Poon, “Silicon and hybrid silicon photonic devices for intra-datacenter applications: state of the art and perspectives,” Photon. Res., vol. 3, pp. B10-B27, October 2015.

[4] W. A. Zortman, A. L. Lentine, D. C. Trotter, and M. R. Watts, “Bit-error-rate monitoring for active wavelength control of resonant modulators,” IEEE Micro, vol. 33, pp. 42-52, January 2013.

[5] H. Jayatilleka, K. Murray, M. A. Guillen-Torres, M. Caverley, R. Hu, N. A. F. Jaeger, L. Chrostowski, and S. Shekhar, “Wavelength tuning and stabilization of microring-based filters using silicon in-resonator photoconductive heaters,” Opt. Express, vol. 23, pp. 25084-25097, September 2015.

[6] Q. Zhu, X. Jiang, Y. Yu, R. Cao, H. Zhang, D. Li, Y. Li, L. Zeng, X. Guo, Y. Zhang, and C. Qiu, “Automated wavelength alignment in a 4 ×4 silicon thermo-optic switch based on dual-ring resonators,” IEEE Photon. J., vol. 10, February 2018.

[7] Q. Zhu, H. Zhang, R. Cao, N. Zhao, X. Jiang, D. Li, Y. Li, X. Song, X. Guo, Y. Zhang, and C. Qiu, “Wide-range automated wavelength calibration over a full FSR in a dual-ring based silicon photonic switch," Proc. of 43rd Opt. Fiber Commun. Conf. (OFC 2018), San Diego (USA), Paper Th3C.1.